


Effects of different effective nucleon-nucleon interactions on α -decay half-life and extracted α -cluster preformation probability

Mingzhao Lu and Niu Wan ^{*}*School of Physics and Optoelectronics, South China University of Technology, Guangzhou 510641, China*

(Received 13 June 2024; accepted 7 October 2024; published 31 October 2024)

Systematical calculations are performed to study the effects of different effective nucleon-nucleon (NN) interactions on α -decay half-life and extracted α -cluster preformation probability. Within the double-folding model, both the nonrelativistic M3Y-type and the relativistic R3Y-type NN interactions are involved and different methods to include the medium effect into the interactions are also introduced. The differences of the effective NN interactions as well as their corresponding nuclear potentials and total α -core potentials are analyzed in detail, and then their impacts on the α -decay half-lives are discussed. By fitting the experimental decay half-lives of α emitters throughout the nuclide chart, three kinds of common α -cluster preformation probability for even-even, odd-A, and odd-odd parent nuclei are extracted within two usual strategies. The obtained values are consistent with previous results and the medium effect on the α -cluster preformation probability is further discussed. Under the extracted preformation probability, the theoretical α -decay half-lives are in good agreement with the experimental data.

DOI: [10.1103/PhysRevC.110.044321](https://doi.org/10.1103/PhysRevC.110.044321)

I. INTRODUCTION

α decay is an important decay mode of unstable nuclei, which can provide abundant nuclear structure information, such as the properties of nuclear ground state, the energy level structure, the valence nucleon interactions, the charge radius, the shell effect, and so on. In 1928, Gamow [1] and independently Gurney and Condon [2] explained the mechanism of α decay by employing the quantum tunneling theory for the first time. Following these pioneering works, different theoretical models were subsequently developed to study the properties of α decay, such as shell model [3,4], generalized liquid drop mode [5], cluster model [6–8], fissionlike model [9,10], a mixture of shell and cluster model [11], and so on. The α -decay process is usually described as the penetration of α cluster preformed in the parent nucleus through the Coulomb barrier of the total interaction between the α cluster and the daughter nucleus. The α -decay width is linked to both the α -cluster preformation probability and the penetration probability through the potential barrier. The former is usually assumed to be unity or extracted from experimental α -decay half-lives, because its fully microscopic calculation involves a complicated many-body system, which is difficult to handle at the present stage. Under certain approximations in the microscopic calculations, the preformation probability can be calculated from the quartetting wave function approach [12] and from the experimental binding energies within the cluster formation model [13,14]. The α -cluster penetration probability is usually calculated by the well-known Wentzel-Kramers-Brillouin (WKB) semiclassical approximation [15–17], and different

α -decay models among the market can well reproduce the orders of magnitude for the experimental α -decay half-lives.

Despite the remarkable theoretical effort, the total interaction between the α cluster and the daughter nucleus remains a large uncertainty, especially for the nuclear potential part. Different nuclear parts of the total α -core potentials have been proposed, such as the phenomenological Woods-Saxon potential [18], the Cosh potential [19], the proximity potential [20–22], the semimicroscopic potential calculated from energy density functional [23,24], the microscopic potential computed from the effective nucleon-nucleon (NN) interactions under the double-folding model (DFM) [25], and so on. Within the DFM by folding the density distributions of both the α cluster and the daughter nucleus to obtain the nuclear potential, there have been many types of effective NN interactions, such as the popular Michigan-3-Yukawa (M3Y) NN interaction [25–30]. The M3Y interaction is developed to fit the G -matrix elements and has been successfully used to study α decay, cluster radioactivity, nucleus-nucleus collision, fusion dynamics, and so on. Based on the M3Y interaction, the density-dependent versions are further constructed to include the medium effect for the involved two-body system with different density-dependent forms, such as BDM3Y, DDM3Y, and CDM3Y [31–33]. The parameters in the density dependence are determined by simulating the equation of state of nuclear matter. These density-dependent NN interactions have also been extensively employed to study the elastic and inelastic collisions for light nuclei as well as α decays.

Besides of the popular M3Y-type NN interactions, the relativistic NN interaction R3Y [34–38] derived from the famous relativistic mean-field theory has been recently used to study the cluster radioactivity [39–41] and fusion reactions [42–44] within the DFM. The corresponding

^{*}Contact author: wanniu@scut.edu.cn

density-dependent version DDR3Y obtained from the relativistic Hartree-Bogoliubov model is also further developed to successfully investigate the medium effect on the fusion reactions [45–47].

Considering the diverse types of the effective NN interactions, it is interesting to compare their different impacts on the double-folding nuclear potential as well as the α -decay half-lives within the DFM. In particular, the relativistic R3Y and DDR3Y NN interactions are rarely employed to study the properties of α decays. In addition, the medium effect within the different effective NN interactions on the α -decay half-lives and the extracted α -cluster preformation probability will also be discussed. This paper is organized as follows. In Sec. II, the details of the theoretical formalism adopted in the present work and the different effective NN interactions are introduced. The corresponding α -decay half-lives and the extracted α -cluster preformation probability are given and discussed in Sec. III. Finally, a summary is given in Sec. IV.

II. THEORETICAL FORMALISM

A. Density-dependent cluster model

The α -decay process is studied within the density-dependent cluster model (DDCM), where the total interaction $V(R)$ between the α cluster and the daughter nucleus can be written as

$$V(R) = V_N(R) + V_C(R) + V_\ell(R), \quad (1)$$

where R is the separation distance between the centers of mass of the α particle and the daughter nucleus, $V_N(R)$ is the nuclear potential, and $V_C(R)$ is the repulsive Coulomb potential. The centrifugal term $V_\ell(R)$ is defined as $V_\ell(R) = \frac{\hbar^2 \ell(\ell+1)}{2\mu R^2}$, where ℓ is the angular momentum carried by the α particle and μ is the reduced mass of the α particle and the daughter nucleus. Within the DFM, the nuclear potential $V_N(R)$ and Coulomb potential $V_C(R)$ can be obtained from the double-folding integral with the density distributions of the α particle and the daughter nucleus [25–27]

$$V_N(R) = \lambda \iint \rho_1(\mathbf{r}_1) \rho_2(\mathbf{r}_2) v_{\text{eff}} d\mathbf{r}_1 d\mathbf{r}_2, \quad (2)$$

$$V_C(R) = \iint \rho_{1p}(\mathbf{r}_1) \rho_{2p}(\mathbf{r}_2) \frac{e^2}{|\mathbf{s}|} d\mathbf{r}_1 d\mathbf{r}_2, \quad (3)$$

where the quantity $|\mathbf{s}|(\mathbf{s} = \mathbf{R} + \mathbf{r}_2 - \mathbf{r}_1)$ is the distance between a nucleon in the α particle and a nucleon in the daughter nucleus. $\rho_1(\mathbf{r}_1)$ and $\rho_2(\mathbf{r}_2)$ are the matter density distributions of α particle and daughter nucleus, while $\rho_{1p}(\mathbf{r}_1)$ and $\rho_{2p}(\mathbf{r}_2)$ are their proton density distributions, respectively. The density distribution of α particle is usually taken as the Gaussian form [25–27]

$$\rho_1(r_1) = 0.4229 \exp(-0.7024r_1^2), \quad (4)$$

and the density distribution of the daughter nucleus is taken as the standard two-parameter Fermi form

$$\rho_2(r_2) = \frac{\rho_0}{1 + \exp\left(\frac{r_2 - c}{a}\right)}, \quad (5)$$

where the half-radius $c = 1.07 A_d^{1/3}$ fm and the diffuseness parameter $a = 0.54$ fm are taken from Refs. [25–27]. The value of ρ_0 is determined by integrating the matter density distribution equivalent to the mass number A_d of the daughter nucleus.

The parameter λ in Eq. (2) is a renormalization factor for the nuclear potential $V_N(R)$, which can be obtained by the Bohr-Sommerfeld (BS) quantization condition [48–50]

$$\int_{R_1}^{R_2} \sqrt{\frac{2\mu}{\hbar^2} [Q - V(R)]} dr = (G - \ell + 1) \frac{\pi}{2}, \quad (6)$$

where R_1 and R_2 as well as the following R_3 are the three classical turning points, which can be obtained by numerical solutions of $V(R) = Q$ with Q being the α -decay energy. The value of the first turning point R_1 is very close to zero since the repulsion from the centrifugal term $V_\ell(R)$ with $\ell \neq 0$ is relatively small. Hence for $\ell = 0$ case with no centrifugal repulsion, it is usually set as $R_1 = 0$, as shown in the following Fig. 1(c) for the α decay $^{212}\text{Po} \rightarrow ^{208}\text{Pb} + \alpha$. The explicit form for the global quantum number G is usually taken as [50]

$$G = \begin{cases} 22 & N > 126, \\ 20 & 82 < N \leq 126, \\ 18 & N \leq 82. \end{cases} \quad (7)$$

Within the two-potential approach [51,52], the α -decay width Γ can be calculated by

$$\Gamma = P_\alpha F \frac{\hbar^2}{4\mu} \exp\left[-2 \int_{R_2}^{R_3} \sqrt{\frac{2\mu}{\hbar^2} |Q - V(R)|} dR\right], \quad (8)$$

where P_α is the preformation probability of the α particle in the parent nucleus. The normalization factor F is obtained by [51,52]

$$F \int_{R_1}^{R_2} \frac{1}{2\sqrt{\frac{2\mu}{\hbar^2} |Q - V(R)|}} dR = 1. \quad (9)$$

The α -decay half-life is then related to the width by the famous relation $T_{1/2} = \hbar \ln 2 / \Gamma$. With the calculated decay half-life T_{cal} by fixing the α -cluster preformation probability as unity, the latter can be extracted from the experimental α -decay half-life T_{exp} [53] by

$$P_\alpha^{\text{cal}} = \frac{T_{\text{cal}}}{T_{\text{exp}}}. \quad (10)$$

From above description about the DDCM, one can find that when the effective NN interaction v_{eff} in Eq. (2) is obtained, we can calculate the nuclear potential as well as the total potential between the α particle and the daughter nucleus. Then the α -decay half-life and the α -cluster preformation probability can be further obtained. Within the DFM for the calculations of the total α -core potential, the M3Y-type NN interactions are widely adopted, such as the M3Y-Reid and M3Y-Paris as well as the density-dependent versions BDM3Y, DDM3Y, and CDM3Y. Recently, the R3Y NN interaction derived from the relativistic mean-field formalism and the corresponding density-dependent version DDR3Y are also used to study the cluster radioactivity and fusion reactions [39–44].

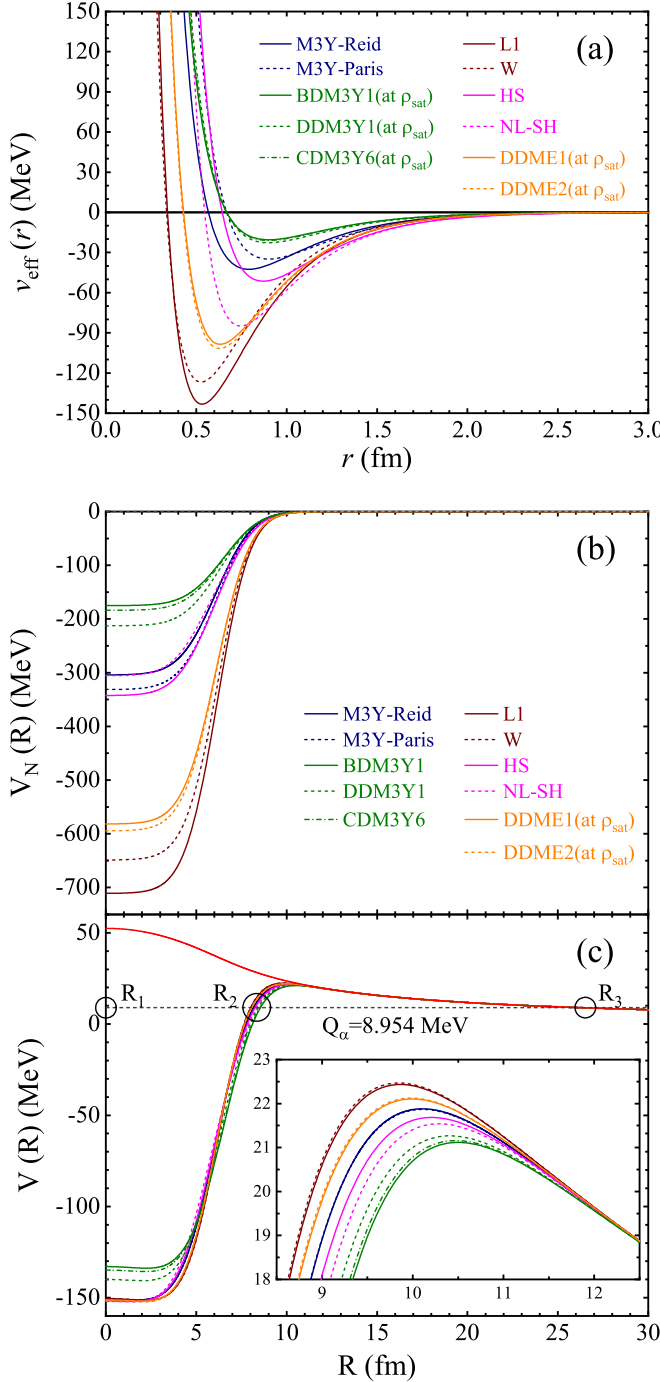


FIG. 1. Different effective NN interactions $v_{\text{eff}}(r)$, the corresponding nuclear potential $V_N(R)$, and the total potential $V(R)$ for the α decay $^{212}\text{Po} \rightarrow ^{208}\text{Pb} + \alpha$ within the DFM.

Next, we will give the explicit forms for these effective NN interactions.

B. M3Y and density-dependent M3Y interactions

The popular M3Y-type NN interaction includes the M3Y-Reid [25] and M3Y-Paris [30] versions, which can be written as

$$v_{\text{eff}}^{\text{R}}(s, E) = 7999 \frac{e^{-4s}}{4s} - 2134 \frac{e^{-2.5s}}{2.5s} + J_{00}^{\text{R}}(E)\delta(s), \quad (11)$$

TABLE I. Values of the parameters in the factor $F(\rho_1, \rho_2)$ for each density-dependent M3Y NN interaction [31–33].

v_{eff}	C	α	$\beta(\text{fm}^3)$	$\gamma(\text{fm}^3)$
BDM3Y1	1.2521	0.0000	0.0000	1.7452
DDM3Y1	0.2963	3.7231	3.7384	0.0000
CDM3Y6	0.2658	3.8033	1.4099	4.0000

$$v_{\text{eff}}^{\text{P}}(s, E) = 11062 \frac{e^{-4s}}{4s} - 2537.5 \frac{e^{-2.5s}}{2.5s} + J_{00}^{\text{P}}(E)\delta(s), \quad (12)$$

where the corresponding zero-range exchange terms are, respectively, given by

$$J_{00}^{\text{R}}(E) = -276(1 - 0.005E/A_\alpha) \text{ MeV fm}^3, \quad (13)$$

$$J_{00}^{\text{P}}(E) = -590(1 - 0.002E/A_\alpha) \text{ MeV fm}^3, \quad (14)$$

where A_α is the mass number of α particle. The density-dependent M3Y NN interaction is constructed to include the medium effect for the involved two-body system, where a density-dependent weight factor is multiplied to the original M3Y-Paris NN interaction as [31–33]

$$v_{\text{eff}}^{\text{DD}}(\rho_1, \rho_2, s, E) = F(\rho_1, \rho_2)v_{\text{eff}}^{\text{P}}(s, E). \quad (15)$$

The explicit form for $F(\rho_1, \rho_2)$ is given as

$$F(\rho_1, \rho_2) = C[1 + \alpha e^{-\beta(\rho_1 + \rho_2)} - \gamma(\rho_1 + \rho_2)], \quad (16)$$

where the parameters C, α, β, γ are determined by reproducing the saturation properties of normal nuclear matter within the Hartree-Fock calculations [31–33]. The $\alpha = 0$ case is usually named as BDM3Y and the $\gamma = 0$ case corresponds to DDM3Y. The CDM3Y version is the hybrid interaction from the former two cases. The values of the parameters C, α, β, γ [31–33] corresponding to BDM3Y1, DDM3Y1, and CDM3Y6 NN interactions are shown in Table I.

C. R3Y and DDR3Y NN interactions

Recently, the R3Y effective NN interaction derived from the relativistic mean-field theory has been successfully used to study the cluster radioactivity and fusion properties within the DFM [39–44]. It is obtained by the summation of the scalar and vector parts of a single meson field, which can be written as [39,40]

$$v_{\text{eff}}^{\text{R3Y}}(s, E) = \frac{g_\omega^2}{4\pi} \frac{e^{-m_\omega s}}{s} + \frac{g_\rho^2}{4\pi} \frac{e^{-m_\rho s}}{s} - \frac{g_\sigma^2}{4\pi} \frac{e^{-m_\sigma s}}{s} + \frac{g_2^2}{4\pi} s e^{-2m_\sigma s} + \frac{g_3^2}{4\pi} \frac{e^{-3m_\sigma s}}{s} + J_{00}(E)\delta(s), \quad (17)$$

where m_ω, m_ρ , and m_σ are the corresponding masses of ω, ρ , and σ mesons. The parameters g_ω, g_ρ , and g_σ are the nucleon-meson coupling constants. g_2 and g_3 denote the nonlinear meson self-interaction parameters. There are various versions of the R3Y NN interactions with different values for above parameters. Within the DFM, the linear version L1, W, and

HS [34–37] and the nonlinear version NL-SH [38] are usually employed. Their explicit forms are given as [34–38]

$$v_{\text{eff}}^{\text{LI}}(s, E) = 9968 \frac{e^{-3.97s}}{4s} - 6661 \frac{e^{-2.79s}}{4s} + J_{00}^{\text{R}}(E)\delta(s), \quad (18)$$

$$v_{\text{eff}}^{\text{W}}(s, E) = 8551 \frac{e^{-3.97s}}{4s} - 5750 \frac{e^{-2.79s}}{4s} + J_{00}^{\text{R}}(E)\delta(s), \quad (19)$$

$$v_{\text{eff}}^{\text{HS}}(s, E) = 11957 \frac{e^{-3.97s}}{4s} + 4099 \frac{e^{-3.90s}}{4s} - 6883 \frac{e^{-2.64s}}{4s} + J_{00}^{\text{P}}(E)\delta(s), \quad (20)$$

and

$$v_{\text{eff}}^{\text{NL-SH}}(s, E) = 10525 \frac{e^{-3.97s}}{4s} + 1207 \frac{e^{-3.87s}}{4s} - 6851 \frac{e^{-2.67s}}{4s} + 2999s \frac{e^{-5.33s}}{4} + 15747 \frac{e^{-7.99s}}{4s} + J_{00}^{\text{P}}(E)\delta(s). \quad (21)$$

It should be mentioned that in the relativistic framework, the medium effect can be introduced by the nonlinear coupling constants, such as the fourth term of above NL-SH version originating from the nonlinear meson self-interaction. In addition, similar to the nonrelativistic M3Y-type NN interactions, the medium effect can also be incorporated in the description of the R3Y NN interaction through the density-dependent nucleon-meson couplings [45–47] without the nonlinear coupling terms. This density-dependent version is named as DDR3Y and the density-dependent couplings are defined as [45–47]

$$g_i(\rho) = g_i(\rho_{\text{sat}})f_i(x)|_{i=\sigma,\omega} \quad (22)$$

with

$$f_i(x) = a_i \frac{1 + b_i(x + d_i)^2}{1 + c_i(x + d_i)^2} \quad (23)$$

and

$$g_\rho(\rho) = g_\rho(\rho_{\text{sat}})\exp[-a_\rho(x - 1)]. \quad (24)$$

Here the parameter $x = \rho/\rho_{\text{sat}}$ is related to the saturation density ρ_{sat} of normal nuclear matter. Thus the DDR3Y NN interaction can be expressed as

$$v_{\text{eff}}^{\text{DDR3Y}}(\rho_1, \rho_2, s, E) = \frac{g_\omega(\rho_1)g_\omega(\rho_2)}{4\pi} \frac{e^{-m_\omega s}}{s} + \frac{g_\rho(\rho_1)g_\rho(\rho_2)}{4\pi} \frac{e^{-m_\rho s}}{s} - \frac{g_\sigma(\rho_1)g_\sigma(\rho_2)}{4\pi} \frac{e^{-m_\sigma s}}{s} + J_{00}^{\text{R}}(E)\delta(s). \quad (25)$$

The parameters a_i , b_i , c_i , d_i , and a_ρ in Eqs. (22)–(24) are determined to fit the properties of finite nuclei and nuclear matter under certain constraints. The parameter sets adopted here are the popular DDME1 [45] and DDME2 [46] versions, which are displayed in Table II.

TABLE II. The parameters for the DDME1 and DDME2 effective NN interactions.

	DDME1 [45]	DDME2 [46]
m_ω (MeV)	783.0000	783.0000
$g_\omega(\rho_{\text{sat}})/\sqrt{\hbar c}$	12.8939	13.0189
a_ω	1.3879	1.3892
b_ω	0.8525	0.9240
c_ω	1.3566	1.4620
d_ω	0.4957	0.4775
m_ρ (MeV)	763.0000	763.0000
$g_\rho(\rho_{\text{sat}})/\sqrt{\hbar c}$	3.8053	3.6836
a_ρ	0.5008	0.5647
m_σ (MeV)	549.5255	550.1238
$g_\sigma(\rho_{\text{sat}})/\sqrt{\hbar c}$	10.4434	10.5396
a_σ	1.3854	1.3881
b_σ	0.9781	1.0943
c_σ	1.5342	1.7057
d_σ	0.4661	0.4421
ρ_{sat} (fm $^{-3}$)	0.152	0.152

III. RESULTS AND DISCUSSION

Within the description of the DDCM for α decays, we can insert the different effective NN interactions into the double-folding integral in Eq. (2) to compute the nuclear potential $V_N(R)$ as well as the total α -core potential $V(R)$. Then the α -decay half-life T_{cal} can be calculated and the α -cluster preformation probability P_α can be extracted with the experimental decay half-life T_{exp} [53]. In order to discuss the effects of different effective NN interactions on α decays, we first show the interactions $v_{\text{eff}}(r)$, the corresponding nuclear potential $V_N(R)$ and the total potential $V(R)$ in Figs. 1(a)–1(c) by taking the α decay $^{212}\text{Po} \rightarrow ^{208}\text{Pb} + \alpha$ with $\ell = 0$ as an example. The effective NN interactions include the density-independent (pure) M3Y-Reid and M3Y-Paris, the density-dependent BDM3Y, DDM3Y, and CDM3Y, the relativistic R3Y interactions L1, W, HS, NL-SH, DDME1, and DDME2. The density-dependent interactions BDM3Y, DDM3Y, CDM3Y, DDME1, and DDME2 are plotted at the saturation density ρ_{sat} . As shown in Fig. 1(a), the attractions of the M3Y-Reid and M3Y-Paris interactions are moderate. However, the repulsion of the latter in small-range region is larger than that of the former, corresponding to the deeper exchange term in Eq. (14) compared with Eq. (13). After the medium effect is further considered, as shown by BDM3Y1, DDM3Y1, and CDM3Y6, more repulsions are included throughout all the ranges. This can also be indicated from Fig. 1(b) that without the renormalization by the BS quantization condition in Eq. (6) ($\lambda = 1$), the nuclear potentials $V_N(R)$ for the density-dependent M3Y interactions are higher than those with pure M3Y types. However, after the renormalization, the total potentials $V(R)$ with the density-dependent M3Y interactions are more repulsive than those with pure M3Y types at small ranges but more attractions are shown in the penetration region. Considering the same Coulomb potential, the barriers with the density-dependent cases are lower than the pure M3Y cases. This can be clearly

TABLE III. Values of the factor λ , the factor F , the classical turning points R_2 and R_3 , the calculated half-life T_{cal} , and the extracted preformation probability P_α for the decay $^{212}\text{Po} \rightarrow ^{208}\text{Pb} + \alpha$ with different effective NN interactions. The first turning point is set as $R_1 = 0$ since the angular momentum carried by the α cluster is $\ell = 0$. The experimental decay energy $Q = 8.954$ MeV and decay half-life $T_{\text{exp}} = 0.294 \times 10^{-6}$ s are taken from Ref. [53].

v_{eff}	λ	F	R_2 (fm)	R_3 (fm)	T_{cal} (s)	P_α
M3Y-Reid	0.669	0.790	8.170	26.375	0.693×10^{-7}	0.235
M3Y-Pairs	0.614	0.795	8.162	26.375	0.699×10^{-7}	0.237
BDM3Y1	1.056	0.733	8.548	26.375	0.188×10^{-7}	0.063
DDM3Y1	0.902	0.750	8.423	26.375	0.273×10^{-7}	0.093
CDM3Y6	1.016	0.740	8.515	26.375	0.206×10^{-7}	0.070
L1	0.284	0.839	8.013	26.374	0.131×10^{-6}	0.447
W	0.311	0.838	8.004	26.374	0.137×10^{-6}	0.467
HS	0.595	0.773	8.248	26.374	0.515×10^{-7}	0.175
NL-SH	0.667	0.755	8.336	26.374	0.386×10^{-7}	0.131
DDME1	0.349	0.818	8.065	26.375	0.100×10^{-6}	0.341
DDME2	0.342	0.820	8.054	26.375	0.104×10^{-6}	0.354

seen from Fig. 1(c), leading to smaller penetration probability and α -decay half-life. Besides, there are very minor differences among the corresponding nuclear potentials $V_N(R)$ and the total potentials $V(R)$ for BDM3Y1, DDM3Y1, and CDM3Y6 cases. This indicates the very similar mechanism for these three nonrelativistic M3Y-type interactions to describe the medium effect.

As for the relativistic R3Y effective NN interactions in Fig. 1(a), the L1 and W interactions possess the strongest attractions with shorter force ranges. Hence their corresponding nuclear potentials $V_N(R)$ in Fig. 1(b) are the deepest. After the renormalization, their total potentials $V(R)$ in Fig. 1(c) provide more attractions at small ranges and less in the penetration region, leading to highest Coulomb barriers. By adding extra repulsive term from ρ meson given in Eq. (20), the HS interaction is very analogous to the pure M3Y types, resulting in very similar nuclear potential and total potential. As mentioned before, there are two methods to include the medium effect for the R3Y NN interaction, namely adding the nonlinear coupling constants such as NL-SH and introducing the density-dependent nucleon-meson couplings such as DDME1 and DDME2. Similarly, the above three interactions can introduce more repulsions compared with the pure R3Y interactions L1 and W, leading to higher nuclear potentials as shown in Fig. 1(b). After the renormalization, the corresponding total potentials provide less attractions at small ranges and more in the penetration region, resulting in lower Coulomb barriers as shown in Fig. 1(c). Moreover, it can be clearly seen from Fig. 1(a) that the NL-SH interaction is very different from the DDME1 and DDME2 interactions. Hence there are also large differences for their nuclear potentials and total potentials. This indicates that these two methods describe the medium effect with very different extent for the R3Y effective NN interactions.

Besides, comparing the nonrelativistic M3Y-type effective NN interactions with the relativistic R3Y types, it can be seen from Fig. 1(a) that the former have moderate attractions, while the latter possess much more attractive forces in smaller ranges. In consequence, the nuclear potentials in Fig. 1(b) for the R3Y types are generally much deeper than

those for the M3Y types. After the renormalization for the total potentials, the R3Y types provide more attractions in small-range region and less in the penetration region than the M3Y types, leading to higher Coulomb barriers and smaller α -decay half-lives. It should be noted that in principle the density distributions of the α particle and the daughter nucleus could be calculated from the effective NN interactions. In order to reduce the uncertainty from calculating the densities, we keep them as the popular forms within the DFM and concentrate on the effects coming from the NN interactions on the α -decay half-life and the extracted α -cluster preformation probability.

In Table III, we give more details about our calculations for the α decay $^{212}\text{Po} \rightarrow ^{208}\text{Pb} + \alpha$, including the values of the renormalization factor λ , the normalization factor F , the second and third turning points R_2 and R_3 , the theoretical decay half-life T_{cal} , and the extracted preformation probability P_α . The first turning point is set as $R_1 = 0$ since the angular momentum carried by the α cluster is $\ell = 0$. From Table III we can see that the values of λ for pure M3Y types are around 0.6, while those for the density-dependent versions are larger and close to unity. This is natural because after the medium effect is included into the density-dependent part, the factor λ possesses less medium effect to renormalize the nuclear potential. The similar trends can also be found from the relativistic R3Y types. However, as mentioned above, since the relativistic R3Y types have much more attractions than the nonrelativistic M3Y types in the inner region, the values of λ are much smaller for the former types. The values of the factor F are all close to unity, indicating the validity of the two-potential approach in Eq. (9). Besides, a common behavior can be obtained for the second turning point R_2 that the values with medium effect are generally larger than others. This originates from the more attractions in the penetration region by the medium effect, leading to lower Coulomb barrier. The third turning points are almost the same because of the short-range nuclear force. As a result, the calculated decay half-life T_{cal} and the extracted preformation probability P_α are smaller by including the medium effect, as shown in the last two columns of Table III.

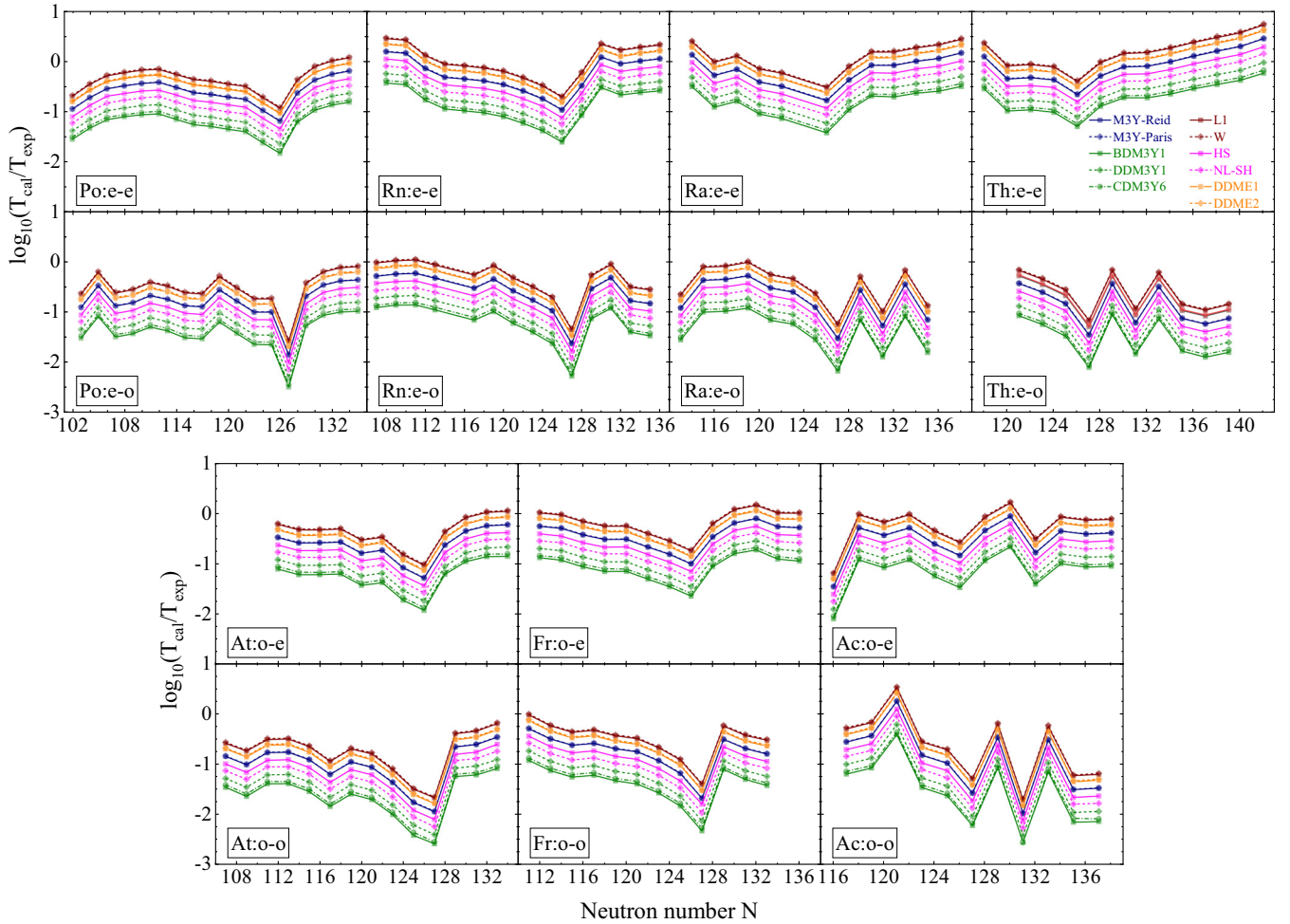


FIG. 2. Deviations of the calculated half-lives from the experimental data for the α emitters in the valley around the two main shells $Z = 82$ and $N = 126$.

In Fig. 2, we show the logarithmic deviations $\log_{10}(T_{\text{cal}}/T_{\text{exp}})$ for the α -decay half-lives T_{cal} calculated with $P_{\alpha} = 1$ compared with the experimental data T_{exp} for the isotopes in the valley around the two main shells $Z = 82$ and $N = 126$. The results in the top panel are for the even- Z isotopes and the bottom panel are for the odd- Z ones. The results from the first row to the last one are successively for the e-e, e-o, odd-even (o-e), and odd-odd (o-o) parent nuclei. It can be seen from Fig. 2 that the numerical sequences of the logarithmic deviation for different effective NN interactions are the same to those of the Coulomb barriers in Fig. 1(c). That is to say, the L1 and W interactions provide the largest absolute logarithmic deviations and the density-dependent M3Y cases give the smallest values. The results of other interactions are between these two cases. This is easy to understand that the penetration probability is decreased with the increasing height and width of the Coulomb barrier, resulting in the increasing α -decay half-life. Hence the higher and wider Coulomb barrier corresponds to the larger calculated α -decay half-life and logarithmic deviation. Moreover, the general behaviors for different effective NN interactions are very similar. That is to say, with the increasing neutron number N of the parent nuclei, the logarithmic deviation is generally decreased before

the closed shell with $N = 126$ and then increased after the closed shell. The shell effect is obviously indicated with the minimal logarithmic deviation around $N = 126$ for even- N parent nuclei and $N = 127$ for odd- N parent nuclei. This is because it is very difficult for the valence nucleons of these two particular nuclei to interact with the ones inside the closed shell to preform α cluster. Hence the preformation probability in these nuclei around the closed shell is relatively small, leading to the smaller calculated α -decay half-lives and the minimal logarithmic deviations. On the contrary, for the parent nuclei with $N = 128$ and $N = 129$, there are large deviation gains due to the increasing α -cluster preformation probability with sufficient valence nucleons outside the closed shell. Moreover, it can also be found from Fig. 2 that the absolute logarithmic deviations for e-e nuclei are generally smaller (around zero) than those for e-o and o-e nuclei, while the latter ones are generally smaller than those for o-o nuclei. This is because with odd protons and odd neutrons, the Pauli blocking effect will hinder the preformation of α cluster, leading to the smaller calculated α -decay half-life and larger logarithmic deviation.

Besides, comparing the results for the density-dependent M3Y interactions with those for the pure M3Y cases, it can

TABLE IV. α -cluster preformation probability P_α extracted with optimized average deviation (AD) and root-mean-square deviation (RD) under different effective NN interactions for e-e, o-A, and o-o parent nuclei, respectively.

v_{eff}	P_α with AD			P_α with RD		
	e-e	o-A	o-o	e-e	o-A	o-o
M3Y-Reid	0.472	0.248	0.129	0.514	0.210	0.109
M3Y-Pairs	0.482	0.253	0.131	0.523	0.214	0.111
BDM3Y1	0.115	0.058	0.034	0.120	0.049	0.026
DDM3Y1	0.172	0.088	0.050	0.184	0.075	0.039
CDM3Y6	0.127	0.064	0.038	0.134	0.055	0.029
L1	0.872	0.453	0.238	0.944	0.390	0.202
W	0.903	0.474	0.246	0.983	0.406	0.211
HS	0.332	0.175	0.092	0.362	0.148	0.077
NL-SH	0.243	0.127	0.069	0.265	0.108	0.056
DDME1	0.675	0.351	0.181	0.726	0.299	0.155
DDME2	0.704	0.366	0.189	0.756	0.311	0.161

be seen that the medium effect reduces the calculated α -decay half-life because of the decreased height and width of the Coulomb barrier, as shown in Fig. 1(c). Similar behavior can also be found from the comparison between the NL-SH interaction and the pure relativistic R3Y cases L1, W, and HS. However, for the DDME1 and DDME2 interactions, the corresponding calculated α -decay half-lives are smaller than those of the deepest L1 and W cases but larger than those of HS case. This is because of the stronger extra repulsion from ρ meson in HS interaction.

In order to study the effects of the different effective NN interactions on the α -cluster preformation probability P_α , we calculate the α -decay half-lives of all the emitters throughout the nuclide chart. Hence we can obtain the preformation probability with Eq. (10). Similar to previous studies, the parent nuclei are also classified into e-e, odd-A (o-A), and o-o cases. By fitting the whole calculated α -decay half-lives to the experimental data, we can extract different common preformation probability for above three kinds of parent nuclei with two usual strategies, namely average deviation (AD) and root-mean-square deviation (RD), which are, respectively, defined as

$$\text{AD} = \frac{1}{M} \sum_{i=1}^M |\log_{10} T_{\text{exp}}^i - \log_{10} T_{\text{cal}}^i|, \quad (26)$$

$$\text{RD} = \sqrt{\frac{1}{M} \sum_{i=1}^M (\log_{10} T_{\text{exp}}^i - \log_{10} T_{\text{cal}}^i)^2}, \quad (27)$$

where M is the number of the involved parent nuclei. By optimizing the values of AD and RD, we obtain three kinds of α -cluster preformation probability P_α under different effective NN interactions. The values are given in Table IV and the comparison for different effective NN interactions are shown in Fig. 3.

From Table IV we can see that under each effective NN interaction, the values of the preformation probability for the e-e nuclei are generally the largest and those for the o-o nuclei

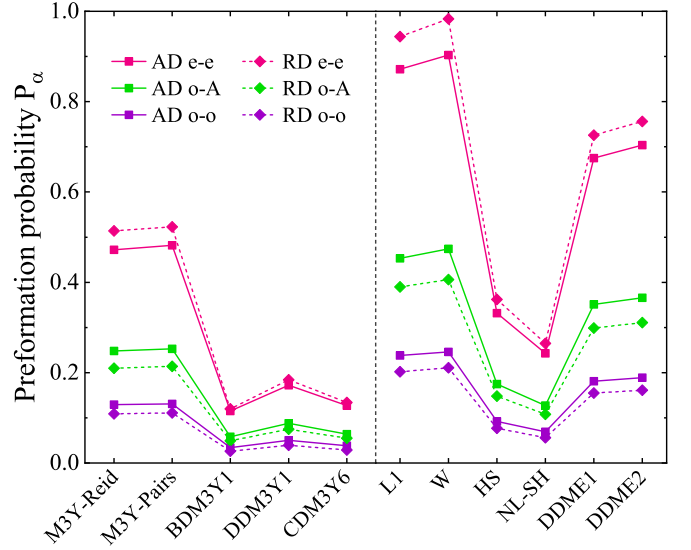


FIG. 3. Comparison for the α -cluster preformation probability under different effective NN interactions.

are the smallest. This is also due to the Pauli blocking effect originating from the odd nucleons. For the pure M3Y-type interactions, our obtained values of the preformation probability are consistent with previous results 0.38, 0.24, and 0.13 [54] for the e-e, o-A, and o-o nuclei, respectively. Besides, it is shown in Table IV that the values of the preformation probability obtained with AD are generally smaller than those with RD for the e-e nuclei, while opposite behavior is for the o-A and o-o nuclei. Moreover, it is clearly shown in Fig. 3 that there are large drops for the values of the preformation probability for all three kinds of nuclei from pure M3Y-type interactions to the density-dependent M3Y types. This is because the density-dependent versions introduce more repulsion in small-range region. As a result, the nuclear interactions between the valence nucleons in the surface region and the daughter nucleus are increased, thus hindering the preformation of α cluster in parent nuclei. Similarly, for the R3Y-type interactions, the values of the preformation probability for all three kinds of nuclei are also decreased from L1 and W to HS, NL-SH, DDME1, and DDME2. Because of the extra repulsion in HS, the corresponding preformation probability are much smaller than those of L1 and W. In addition, the values for NL-SH and DDME1/DDME2 are also very different, which is because of the different methods to include the medium effect. For the NL-SH interaction, the medium effect is introduced by adding the nonlinear coupling constants. As a result, there are more attractions in the penetration region, leading to lower Coulomb barrier and smaller calculated α -decay half-life as well as the extracted preformation probability. On the contrary, the DDME1 and DDME2 introduce the density-dependent nucleon-meson couplings to describe the medium effect, which results in less attractions in the penetration region and higher Coulomb barrier. Hence the calculated α -decay half-life and the extracted preformation probability are increased a lot. In the future, more detailed studies are necessary to include the medium effect for the

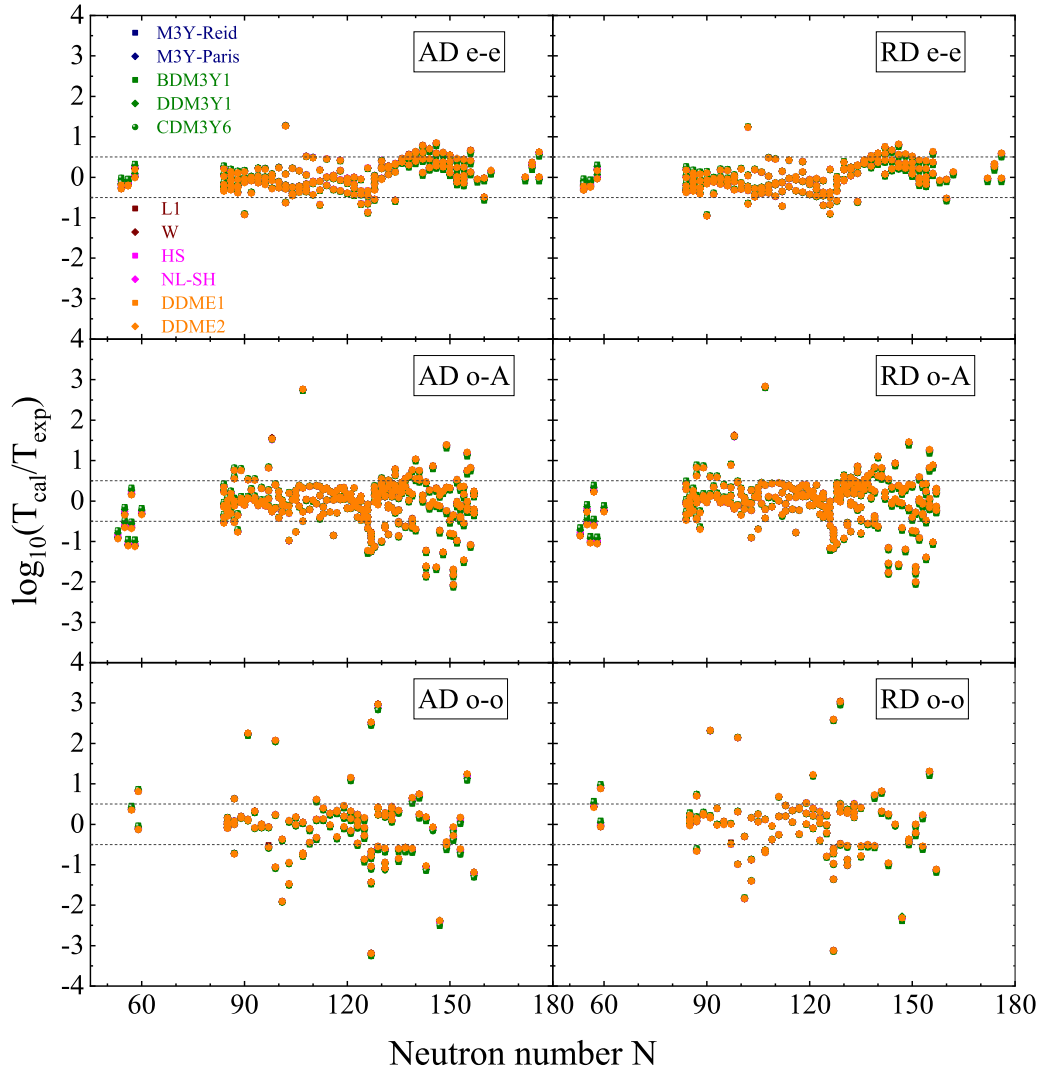


FIG. 4. Comparison for the calculated α -decay half-lives with the experimental data by using the extracted α -cluster preformation probability.

effective NN interactions. Compared the M3Y-type interactions with the R3Y types, it can be seen from Fig. 3 that the values of the preformation probability are generally consistent with each other for all three kinds of parent nuclei. The differences are within a reasonable range despite the deepest L1 and W interactions provide a little larger preformation probability.

With the extracted preformation probability given in Table IV, we recalculate the α -decay half-lives for all the α emitters throughout the nuclide chart. The comparison for the calculated α -decay half-lives with the experimental data are shown in Fig. 4. It can be clearly seen from Fig. 4 that with the extracted preformation probability, the logarithmic deviations of the α -decay half-lives are all generally in the range ± 0.5 . That is to say, the calculated α -decay half-lives are consistent with the experimental data within a factor of 3. Considering the complicated couplings from the odd nucleons, the distributions for the o-o nuclei are a little larger than other two types of nuclei. Besides, the deviation distributions for AD are in good agreement with those for RD, indicating the consistent

mechanism for these two strategies to extract the α -cluster preformation probability.

IV. SUMMARY

Within the double-folding model (DFM), we insert various effective nucleon-nucleon (NN) interactions to compute the nuclear potentials between the α cluster and the daughter nucleus, including the nonrelativistic M3Y types and the relativistic R3Y types as well as their extended versions including the medium effect. We first compare the different effective NN interactions as well as their corresponding nuclear potential and total potential in detail. By including the medium effect, more repulsions are generally introduced compared with the pure versions, resulting lower Coulomb barriers and smaller α -decay half-lives. With the experimental decay half-lives for even-even, odd-A, and odd-odd parent nuclei throughout the nuclide chart, we extract different common α -cluster preformation probability for different effective NN interactions under two usual strategies. Generally, the values

of the preformation probability with including the medium effect are smaller than those of the pure versions. The obtained values for the M3Y-type interactions are consistent with those for the R3Y types and also agree with previous studies. In addition, there are differences for the two methods to include the medium effect in R3Y-type interactions. Moreover, with the extracted preformation probability, the calculated α -decay half-lives for all the α emitters are in good agreement with the experimental data, especially for the even-even parent nuclei.

ACKNOWLEDGMENTS

This work was supported by the National Natural Science Foundation of China (Grants No. 12205105 and No. 12311540139), by the Fundamental and Applied Fundamental Research Program of Guangzhou (Grant No. 2023A04J1311), by the Fundamental Research Funds for the Central Universities (Grant No. 2024ZYGXZR058) and the startup funding of the South China University of Technology.

-
- [1] G. Gamow, *Z. Phys.* **51**, 204 (1928).
 - [2] R. W. Gurney and E. U. Condon, *Nature (London)* **122**, 439 (1928).
 - [3] H. J. Mang, *Phys. Rev.* **119**, 1069 (1960).
 - [4] V. G. Soloviev, *Phys. Lett.* **1**, 202 (1962).
 - [5] G. Royer, C. Normand, and E. Druet, *Nucl. Phys. A* **634**, 267 (1998).
 - [6] B. Buck, A. C. Merchant, and S. M. Perez, *Phys. Rev. C* **45**, 2247 (1992).
 - [7] B. Buck, A. C. Merchant, and S. M. Perez, *At. Data Nucl. Data Tables* **54**, 53 (1993).
 - [8] P. Mohr, *Phys. Rev. C* **73**, 031301(R) (2006).
 - [9] D. N. Poenaru, I. H. Plonski, and W. Greiner, *Phys. Rev. C* **74**, 014312 (2006).
 - [10] P. R. Chowdhury, C. Samanta, and D. N. Basu, *Phys. Rev. C* **73**, 014612 (2006).
 - [11] K. Varga, R. G. Lovas, and R. J. Liotta, *Phys. Rev. Lett.* **69**, 37 (1992).
 - [12] C. Xu, Z. Ren, G. Röpke, P. Schuck, Y. Funaki, H. Horiuchi, A. Tohsaki, T. Yamada, and B. Zhou, *Phys. Rev. C* **93**, 011306(R) (2016).
 - [13] S. M. Saleh Ahmed, R. Yahaya, S. Radiman, and M. S. Yasir, *J. Phys. G* **40**, 065105 (2013).
 - [14] D. Deng, Z. Ren, D. Ni, and Y. Qian, *J. Phys. G* **42**, 075106 (2015); D. Deng and Z. Ren, *Phys. Rev. C* **93**, 044326 (2016).
 - [15] H. Jeffreys, *Proc. London Math. Soc.* **s2-23**, 428 (1925).
 - [16] H. A. Kramers, *Z. Phys.* **39**, 828 (1926).
 - [17] G. Wentzel, *Z. Phys.* **38**, 518 (1926).
 - [18] R. D. Woods and D. S. Saxon, *Phys. Rev.* **95**, 577 (1954).
 - [19] B. Buck, A. C. Merchant, and S. M. Perez, *Phys. Rev. Lett.* **72**, 1326 (1994); **76**, 380 (1996).
 - [20] J. Błocki, J. Randrup, W. J. Swiatecki, and C. F. Tsang, *Ann. Phys. (NY)* **105**, 427 (1977).
 - [21] K. P. Santhosh, S. Sabina, and R. K. Biju, *Nucl. Phys. A* **825**, 159 (2009).
 - [22] J. G. Deng, J. C. Zhao, P. C. Chu, and X. H. Li, *Phys. Rev. C* **97**, 044322 (2018).
 - [23] F. L. Stancu and D. M. Brink, *Nucl. Phys. A* **270**, 236 (1976).
 - [24] W. M. Seif, *Eur. Phys. J. A* **38**, 85 (2008).
 - [25] G. R. Satchler and W. Love, *Phys. Rep.* **55**, 183 (1979).
 - [26] G. F. Bertsch, J. Borysowicz, H. McManus, and W. G. Love, *Nucl. Phys. A* **284**, 399 (1977).
 - [27] C. Xu and Z. Ren, *Nucl. Phys. A* **760**, 303 (2005).
 - [28] A. M. Kobos, B. A. Brown, P. Hodgson, G. R. Satchler, and A. Budzanowski, *Nucl. Phys. A* **384**, 65 (1982).
 - [29] A. M. Kobos, B. A. Brown, R. Lindsay, and G. R. Satchler, *Nucl. Phys. A* **425**, 205 (1984).
 - [30] M. Lacombe, B. Loiseau, J. M. Richard, R. Vinh Mau, J. Côté, P. Pirès, and R. de Tourreil, *Phys. Rev. C* **21**, 861 (1980).
 - [31] D. T. Khoa, W. von Oertzen, and H. G. Bohlen, *Phys. Rev. C* **49**, 1652 (1994).
 - [32] D. T. Khoa and W. Von Oertzen, *Phys. Lett. B* **342**, 6 (1995).
 - [33] D. T. Khoa, G. R. Satchler, and W. von Oertzen, *Phys. Rev. C* **56**, 954 (1997).
 - [34] C. J. Horowitz and B. D. Serot, *Nucl. Phys. A* **368**, 503 (1981).
 - [35] B. D. Serot and J. D. Walecka, *Int. J. Mod. Phys. E* **6**, 515 (1997).
 - [36] P. G. Reinhard, *Rep. Prog. Phys.* **52**, 439 (1989).
 - [37] S. K. Patra and C. R. Praharaj, *Phys. Rev. C* **44**, 2552 (1991).
 - [38] G. A. Lalazissis, J. König, and P. Ring, *Phys. Rev. C* **55**, 540 (1997).
 - [39] B. Singh, M. Bhuyan, S. K. Patra, and R. K. Gupta, *J. Phys. G: Nucl. Part. Phys.* **39**, 025101 (2012).
 - [40] C. Lahiri, S. K. Biswal, and S. K. Patra, *Int. J. Mod. Phys. E* **25**, 1650015 (2016).
 - [41] B. Kunwar, A. Bhadra, and S. K. Sen Gupta, *Phys. Rev. C* **84**, 034614 (2011).
 - [42] M. Bhuyan and R. Kumar, *Phys. Rev. C* **98**, 054610 (2018).
 - [43] S. Rana, R. Kumar, and M. Bhuyan, *Phys. Rev. C* **104**, 024619 (2021).
 - [44] R. Kumar, S. Rana, M. Bhuyan, and P. Mohr, *Phys. Rev. C* **105**, 044606 (2022).
 - [45] T. Nikšić, D. Vretenar, P. Finelli, and P. Ring, *Phys. Rev. C* **66**, 024306 (2002).
 - [46] G. A. Lalazissis, T. Nikšić, D. Vretenar, and P. Ring, *Phys. Rev. C* **71**, 024312 (2005).
 - [47] M. Bhuyan, S. Rana, N. Jain, R. Kumar, S. K. Patra, and B. V. Carlson, *Phys. Rev. C* **106**, 044602 (2022).
 - [48] B. Buck, A. C. Merchant, S. M. Perez, and P. Tripe, *Phys. Rev. C* **47**, 1307 (1993).
 - [49] B. Buck, J. C. Johnston, A. C. Merchant, and S. M. Perez, *Phys. Rev. C* **53**, 2841 (1996).
 - [50] C. Xu and Z. Ren, *Phys. Rev. C* **69**, 024614 (2004).
 - [51] S. A. Gurvitz and G. Kalbermann, *Phys. Rev. Lett.* **59**, 262 (1987).
 - [52] S. A. Gurvitz, *Phys. Rev. A* **38**, 1747 (1988).
 - [53] F. G. Kondev, M. Wang, W. J. Huang, S. Naimi, and G. Audi, *Chin. Phys. C* **45**, 030001 (2021); W. J. Huang, M. Wang, F. G. Kondev, G. Audi, and S. Naimi, **45**, 030002 (2021).
 - [54] C. Xu and Z. Ren, *Phys. Rev. C* **74**, 014304 (2006).